Journal of Hazardous Materials 201–202 (2012) 185–192

Contents lists available at SciVerse ScienceDirect

Journal of Hazardous Materials

journal homepage: www.elsevier.com/locate/jhazmat

Conversion of emitted dimethyl sulfide into eco-friendly species using low-temperature atmospheric argon micro-plasma system

Hsin-Hung Chen[a], Chih-Chiang Weng[a,b], Jiunn-Der Liao[a,b,*], Liang-Ming Whang[c,d], Wei-Hung Kang[e]

[a] Department of Materials Science and Engineering, National Cheng Kung University, 1 University Road, Tainan City 70101, Taiwan
[b] Promotion Center for Global Materials Research, National Cheng Kung University, 1 University Road, Tainan City 70101, Taiwan
[c] Department of Environmental Engineering, National Cheng Kung University, 1 University Road, Tainan City 70101, Taiwan
[d] Research Center for Energy Technology and Strategy, National Cheng Kung University, 1 University Road, Tainan City 70101, Taiwan
[e] Chimei Innolux Corporation, Southern Taiwan Science Park, 3 Huansi Rd. Sec. 1, Tainan City 74147, Taiwan

ARTICLE INFO

Article history:
Received 29 June 2011
Received in revised form 15 October 2011
Accepted 19 November 2011
Available online 28 November 2011

Keywords:
Atmospheric argon micro-plasma system
Dimethyl sulfide
Decomposition
Treatment efficiency
Recycling

ABSTRACT

A custom-made atmospheric argon micro-plasma system was employed to dissociate dimethyl sulfide (DMS) into a non-foul-smelling species. The proposed system takes the advantages of low energy requirement and non-thermal process with a constant flow rate at ambient condition. In the experiments, the compositions of DMS/argon plasma, the residual gaseous phases, and solid precipitates were respectively characterized using an optical emission spectrometer, various gas-phase analyzers, and X-ray photoemission spectroscopy. For 400 ppm DMS introduced into argon plasma with two pairs of electrodes (90 W), a complete decomposition of DMS was achieved; the DMS became converted into excited species such as C^*, C_2^*, H^*, and CH^*. When gaseous products were taken away from the treatment area, the excited species tended to recombine and form stable compounds or species, which formed as solid particles and gaseous phases. The solid deposition was likely formed by the agglomeration of C-, H-, and S-containing species that became deposited on the quartz inner tube. For the residual gaseous phases, low-molecular-weight segments mostly recombined into relatively thermodynamic stable species, such as hydrogen, hydrogen sulfide, and carbon disulfide. The dissociation mechanism and treatment efficiency are discussed, and a treatment of converting DMS into H_2-, CS_2-, and H_2S-dominant by-products is proposed.

1. Introduction

Volatile organic sulfur compounds (VOSCs) have recently been assigned important roles in the global sulfur cycle (a combination of biological, chemical, and geochemical processes). VOSCs have important environmental functions related to global warming, acid precipitation, and cloud formation. A major component of the VOSC group is dimethyl sulfide (DMS, CH_3–S–CH_3) [1]. DMS has an unpleasant smell with a low olfactory threshold (0.02–0.1 ppm).

A number of organic compounds, such as photoresists and solvents, are widely utilized in industry. The utilization of organic compounds creates a substantial amount of pollutant by-products that raise environmental concerns [2]. Volatile organic compounds (VOCs) and solvents, e.g., dimethyl sulfoxide (DMSO), are often necessary for thin-film transistor liquid crystal display (TFT-LCD) processing. DMSO is widely used as a solvent, lubricant, preservative, or stabilizer in a number of industrial, agricultural, and pharmaceutical applications [3,4]. Although DMSO itself has low toxicity, its main by-product from the reduction reaction, DMS, is volatile and noxious in nature. DMS particles, which have a long adhesion time, seriously affect the cleanliness of the semiconductor manufacturing process and dramatically reduce the production yield. DMS treatment is thus an environmental control issue.

DMS can be typically treated by catalytic incineration [5]. However, this consumes a lot of energy and generates secondary pollution. For example, wet scrubbers have a high efficiency, but require costly oxidizing chemicals (e.g., ClO_2). Potentially, they can produce chlorinated hydrocarbons if not properly controlled [6]. Thermal oxidation implies high energy consumption for greatly diluted effluents. Adsorption processes using activated carbon are non-destructive techniques and result in the use of expensive secondary treatment processes [7]. Plasma torch at atmospheric pressure is a promising alternative to conventional thermal combustion processes; it requires no electrodes and produces high electron, ion, and radical densities. The decomposition of halogenated VOCs with thermal plasma sources has been performed [8]. The maximum gas temperature of a plasma torch may reach ≈4000 K [8] and achieve a complete decomposition of VOCs or

* Corresponding author at: Department of Materials Science and Engineering, National Cheng Kung University, 1 University Road, Tainan City 70101, Taiwan. Tel.: +886 6 2757575x62971; fax: +886 6 2346290.
E-mail address: jdliao@mail.ncku.edu.tw (J.-D. Liao).

0304-3894/$ – see front matter © 2011 Elsevier B.V. All rights reserved.
doi:10.1016/j.jhazmat.2011.11.064

gaseous sulfide compounds with an energy density of ≈1000 J/cm^3 [9]. Thermal plasma is effective in decomposing dense VOCs due to its high temperature; however, it is still not economical for the decomposition of dilute VOCs.

Low-pressure plasma has been applied to reduce VOSCs such as carbon disulfide, methanethiol, and DMS due to its relatively low energy consumption and high treatment efficiency [10,11]. VOSCs can be decomposed at room temperature using a radio-frequency (RF) argon plasma reactor under low pressure. The decomposition efficiency increases with increasing applied power and oxygen content [12]. However, low-pressure plasma systems usually require an expensive vacuum apparatus for batch treatment.

Non-thermal atmospheric plasma systems operating at high voltage and low current are a promising alternative for the treatment of VOSCs. The systems are usually based on dielectric barrier discharge (DBD) or pulsed corona discharge (PCD) [13]. The former technique has some practical advantages, such as being a relatively low-temperature process and having high decomposition efficiency for the decomposition of VOCs [14]. Due to low energy efficiency, the combination of DBD and catalysts is frequently applied for decomposing VOCs [15]. Nevertheless, the application of catalysts may lead to secondary pollution. PCD has been used for the decomposition of gaseous sulfide compounds [7,16,17]. Removal and destruction efficiencies of ≈99% can be obtained with power levels ranging from 0.1 to 0.3 J/cm^3, which are competitive with those obtained using existing technologies. However, PCD reactors use a wire-in-cylinder design; an inner electrode is usually used in the apparatus. The attachment of reactive gases onto the inner electrode tends to corrode it, reducing the efficiency of the reactor with operation time.

Atmospheric-pressure micro-plasma technology, e.g., micro-plasma reactors based on capillary electrode discharge (CPE), has remarkable stability, which can be explained by Paschen's Law [18], and low energy consumption for the study of VOC destruction [19]. CPE uses capillary jet mode, which produces jets of high-intensity plasma at atmospheric pressure. Maximum VOC destruction efficiencies of 80–100% can be obtained with an energy density of 2 J/cm^3 for most compounds studied. The decomposition of several prototypical aliphatic (e.g., ethylene, heptane, octane) and aromatic (e.g., benzene, toluene, ethylbenzene, xylene) compounds as well as ammonia has been studied [18,20].

Micro-plasma technology has a low breakdown voltage and a low energy requirement with high output plasma density. Table 1 of Appendix A shows a comparison of plasma parameters for various atmospheric plasma sources. To prevent the PCD-type electrode from corroding, a custom-made RF-driven micro-plasma system, which is a type of micro-plasma jet containing two outer electrodes, is applied for the decomposition of DMS. A RF-driven plasma jet maintains non-thermal properties by preventing glow-to-arc transitions via an oscillating electric field and the inclusion of rare gases in the reactor process stream to prevent discharge instabilities [21]. In the experiment, argon, which has a relatively low breakdown voltage and is an atomic gas, was employed as the buffer gas. A probable mechanism of DMS decomposition as a function of treatment time at atmospheric pressure is presented.

2. Experimental

2.1. Micro-plasma system with the mixture of ca DMS in argon

A schematic diagram of the experimental setup is shown in Fig. 1(a). The setup mainly consists of a micro-plasma reactor, a DMS feeding system, and a 13.56 MHz RF power supply (maximum input: 325 W, ACG-3B, MKS *ENI Corp.*, Rochester, USA) with a matching network (MW-5DM11, *ENI Corp.*, Rochester, USA). The micro-plasma system is a type of micro-plasma jet system, which contains a quartz tube as the gas channel and a dielectric layer. The outer and inner diameters of the tube are ≈3.0 and ≈1.5 mm, respectively. To prevent the reactant gas from becoming attached to the inner electrode, which may reduce efficiency, two outer electrodes are designated for the dissociation of DMS in argon.

Copper tape pasted on the outer surface of a capillary quartz tube (width: 6.4 mm; thickness: 0.06 mm, *Electron Microscopy Sciences*, PA, USA) was employed as the electrode. One of the electrodes near the gas inlet was connected to the output of the RF power supply; the other electrode near the gas outlet was connected to the ground (configuration is shown in Fig. 1(b); this type of configuration is denoted as "one pair of electrodes" hereafter). The micro-plasma was stably ignited and maintained; the gap between the two electrodes was kept at ≈3.0 mm with the applied power was 40 W. For this gap, the effective treatment volume was ≈27.7 mm^3. Therefore, the average treatment time per DMS molecule was ≈6.7×10^{-4} s for a flow rate of 2500 sccm. Under this condition, the maximum concentration of DMS which can be added into argon micro-plasma was ≈400 ppm. Commercially available DMS (99.9%, CAS number: 75-18-3, *Merck*, Germany) was utilized in the experiment. To obtain a suitable concentration (i.e., ≈400 ppm) of DMS, high-purity argon (99.99%, *Yun-Hai Co., Ltd.*, Taiwan) was used as both the buffer gas and the carrier gas to pass through a DMS container; the DMS was kept at −78 °C in a cooling system with alcohol as the media. The dissociation mechanism of DMS under these conditions is discussed in Section 3.4. To determine the influence of treatment time and input power, series of two pairs of electrodes (this type of configuration is denoted as "two pairs of electrodes" hereafter), as shown in Fig. 1(c), was designated for the decomposition of DMS. The reaction time, up to 1.34×10^{-3} s, of the DMS sample was expected to be doubled compared to that of one pair of electrodes.

2.2. Analysis of residual gas after plasma treatment

Before plasma treatment, 400 ppm DMS/argon was collected as the control. After igniting 400 ppm DMS/argon plasma and lasting for 10 min (i.e., until the plasma became stable), the residual gas was collected using a gas sampler and a 700 ml sampling bag (232-945A, *SKC Inc.*, PA, USA) from the sampling exit, as indicated by the single asterisk in Fig. 1(a).

The variation of sulfide with plasma treatment was estimated using a gas chromatography/flame photometric detector (GC-FPD, GC-2014, *Shimadzu Corp.*, Japan) combined with a GS-Q column (30 m × 0.53 m), which is typically employed to analyze the compositional change of sulfide and phosphide. A gas chromatography/thermal conductivity detector (GC-TCD) was employed to examine the by-products derived from hydrogen or hydrocarbon molecules. A Fourier transform infrared spectrometer (FTIR, Nexus 470, *Thermo Nicolet*, USA) combined with a transmittance-type 9.6 m gas cell was applied to analyze the gaseous compositions after micro-plasma treatment.

2.3. Optical diagnosis of excited species

The excited species in argon and DMS/argon micro-plasma were detected using a single monochromator (SpectraPro 2300i, *Princeton Instruments,* New Jersey, USA) equipped with a charge-coupled detector (CCD, 1340 × 100 pixels, NTE: 100B, *Princeton Instruments*, New Jersey, USA). The CCD resolution is ≈0.14 nm. The head of the optical fiber used for detecting light emissions was placed side-on ≈12 mm away from the discharge zone between the two electrodes to record the real-time emission spectrum with one pair of electrodes (40 W), as shown in Fig. 1(a). The focal length of the monochromator is ≈300 mm. Two gratings were used: 200–500 nm (1200 g/mm) and 500–1100 nm

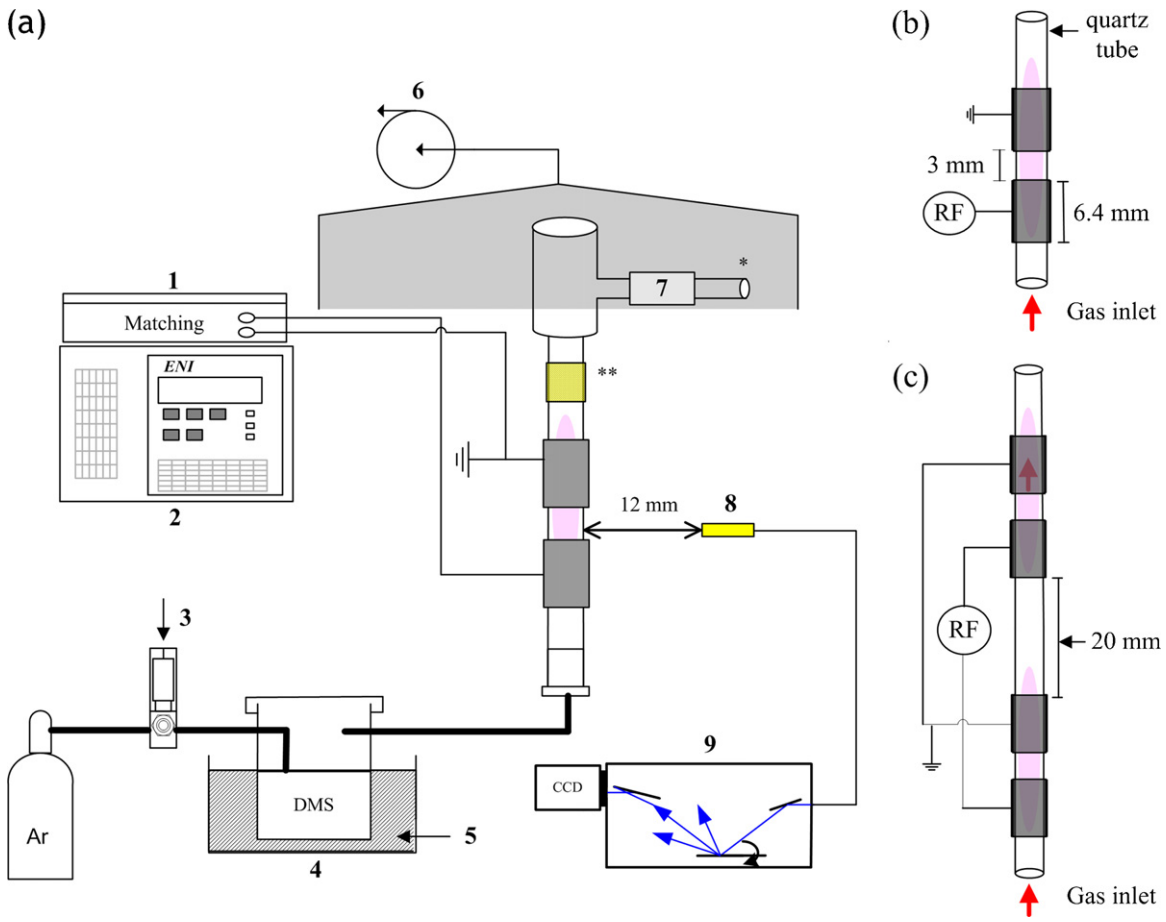

Fig. 1. (a) Illustration of experimental set-up of RF atmospheric Ar micro-plasma system for the decomposition of DMS. (1) Matching network, (2) RF power supply, (3) mass flow controller, (4) cooling system, (5) alcohol as media, (6) air-extracting apparatus, (7) valve, (8) fiber head, (9) monochromator; schemes of (b) one pair of electrodes and (c) two pairs of electrodes micro-plasma systems.

(1200 g/mm). The spectral resolution of the collection was ≈0.1 nm with the 1200 g/mm grating. A mercury lamp (MS-416, *Princeton Instruments*, USA) was used for the calibration of the wavelength. During the diagnostic procedures, the width of entrance slit was kept constant at l0 μm and the exposure time was 0.01 s. A strong argon atomic (Ar-I, 4p–4s) spectrum was observed in the range of 700–900 nm, and carbon-related molecules were detectable in the range of 300–700 nm. Note that the carbon-related molecules may provide considerable information about the residual products after DMS/argon plasma treatment.

2.4. Analysis of solid deposition on the quartz tube in the afterglow region

The morphology study and elemental analysis of the deposited solid products were conducted using a high-resolution thermal field-emission scanning electron microscope (FE-SEM, JSM-7001, *JEOL*, Japan) combined with an energy dispersive X-ray spectrometer (EDS). Further chemical analyses on the products were respectively conducted using X-ray photoelectron spectroscopy (XPS, PHI 5000 VersaProbe, *ULVAC-PHI Inc.*, Japan) and FTIR. XPS was performed using a monochromatic Al-Kα source (25 W, $h\nu$ = 1486.6 eV) with an energy resolution of ≈0.49 eV. All XPS spectra were obtained at a take-off angle of 45° for each element. A wide-scan spectrum and fine-scan spectra in the O 1s, S 2p, C 1s, Si 2p and N 1s regions were measured. FTIR measurements were performed using a spectrometer (Spectrum GX, *PerkinElmer*, USA) with the resolution of 4 cm^{-1} in the scanning range of 4000–400 cm^{-1}.

3. Results and discussion

3.1. Real-time observation of DMS/argon plasma state

In Fig. 1(b) and (c), the excited state of pure argon plasma with a one pair of electrodes and two pairs of electrodes exhibits a light purple color. The emissions from Ar-I in a large wavelength range of 650–875 nm, namely the atomic oxygen (O-I, $3p^5P - 3s^5S$), the Balmer line H_α (3d–2p), and the OH band ($A^2\Sigma^+ \rightarrow X^2\Pi_g$), are shown in Fig. 2(a) (i) and (b) (i) [22]. As 400 ppm DMS was introduced into the argon plasma, the emission color became mostly green. As shown in Fig. 2(a) (ii), the intensity of Ar-I was dramatically reduced in DMS/argon plasma compared to that of Ar-I in pure argon plasma (Fig. 2(a) (i)). The peak intensity at 750.4 nm (i.e., in the Ar-I region) was taken as the reference.

The emission range of 200–680 nm in Fig. 2(a) is enlarged in Fig. 2(b). In addition to Ar-I, H_α, and OH bands, C-derived species such as atomic C (C-I), C_2, CH, and CN were detected [23]. The Swan band system ($A^3\Pi_g - X'^3\Pi_u$ transition) of the C_2 molecule has several molecular vibrational bands in the visible spectral range. The most prominent one is the $\nu' = \nu'' = 0$ transition with a band head at 516.5 nm. These C_2 bands, which are frequently found in sources containing carbon, contributed to the green part of the flame or discharge. This is consistent with the appearance of discharge shift green in the DMS/argon plasma. The CH dominant molecular band

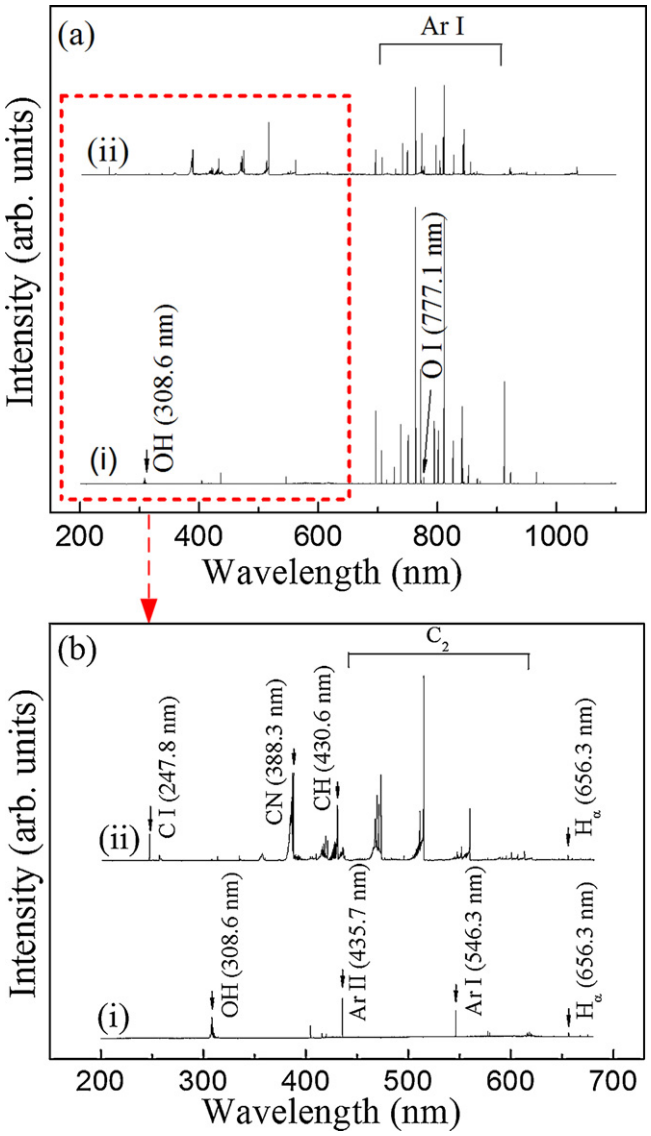

Fig. 2. (a) Real-time optical emission spectra of (i) argon and (ii) DMS/argon micro-plasma for one pair of electrodes at 40 W; (b) enlargement in the range of 200–680 nm.

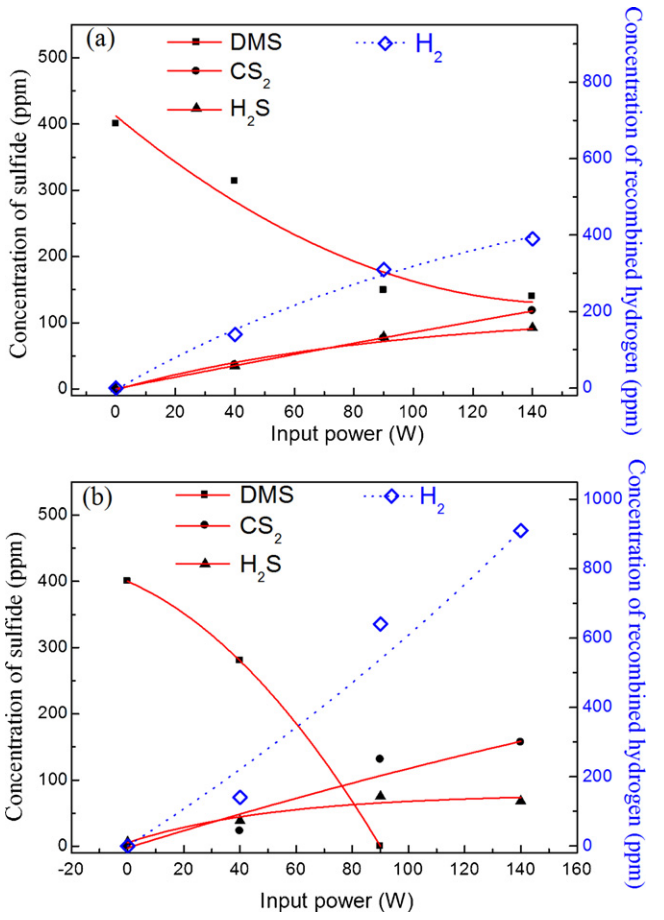

Fig. 3. Concentrations of DMS, H_2S, and CS_2 and the yield of hydrogen as functions of applied RF power (0, 40, 90, and 140 W) for (a) one pair of electrodes and (b) two pairs of electrodes micro-plasma systems.

at 430.6 nm originates from the $A^2\Delta - X^2\Pi$ transition with the band head, degrading 10 nm to the violet. The CN radical originates from the $B^2\sum - X^2\Pi$ transition with band heads at 388.3 and 421.6 nm, respectively.

Presumably, the N-containing excited species were generated by the recombination of residual excited species with air in the afterglow region, whereas the O-containing species formed in the discharge region and combined with air in the afterglow region. As shown in Fig. 2(b) (ii), the intensity of the OH bands decreased dramatically as 400 ppm DMS was added into the argon micro-plasma with one pair of electrodes (40 W). Carbon-related fragments resulted from the dissociation of DMS. The OH band is attributed by the excited argon to follow the quenching mechanisms of OH ($A^2\Sigma^+$) [24], dominated by an energy transfer process between few H_2O from atmosphere and the excited (or metastable) argon species (the energy carried by the argon metastables Ar (4s) is around 11.5–11.7 eV). As 400 ppm DMS was added into the argon plasma, the energy of electron or the excited (or metastable) argon species was mostly transferred to the dissociation of DMS molecules due to their relatively low dissociation energies (as indicated in Appendix B) comparing to that of H_2O (≈9.1 eV) [24]. The elementary processes in the DMS/argon plasma are therefore correlated with the excitation/recombination of the argon plasma, the dissociation of DMS molecules, and the humidity of the ambient air.

3.2. Variation of residual species in DMS/argon plasma with input power

Residual gases and related by-products were analyzed by GC-FPD and GC-TCD, respectively. Before the measurements, the flow rate of the DMS/argon plasma and the reaction durations for the one pair and two pairs of electrodes were optimized. To test the efficiency of DMS treatment, the input power for the DMS/argon plasma was increased from 40 to 90 and 140 W, respectively.

The yield of recombined hydrogen as a function of the input power for the DMS/argon micro-plasma for one pair and two pairs of electrodes, respectively, was measured by GC-TCD. The results are shown in Fig. 3(a) and (b). For DMS/argon micro-plasma with one pair and two pairs of electrodes, the yields of recombined hydrogen increased from 140 (40 W) to 390 and 910 ppm (140 W), respectively. The results indicate that the recombination of excited hydrogen atoms (e.g., H^*) into hydrogen gas increased with increasing input power and DMS/argon reaction time.

The residual gas was also analyzed by FTIR with a 9.6 m gas cell. The spectra are given in Appendix C. From the rotational–vibrational spectrum of carbon monoxide (CO) gas, the presence of P- and R- branches (e.g., centered at about 2143 cm^{-1}) imply that active O atoms from the atmosphere

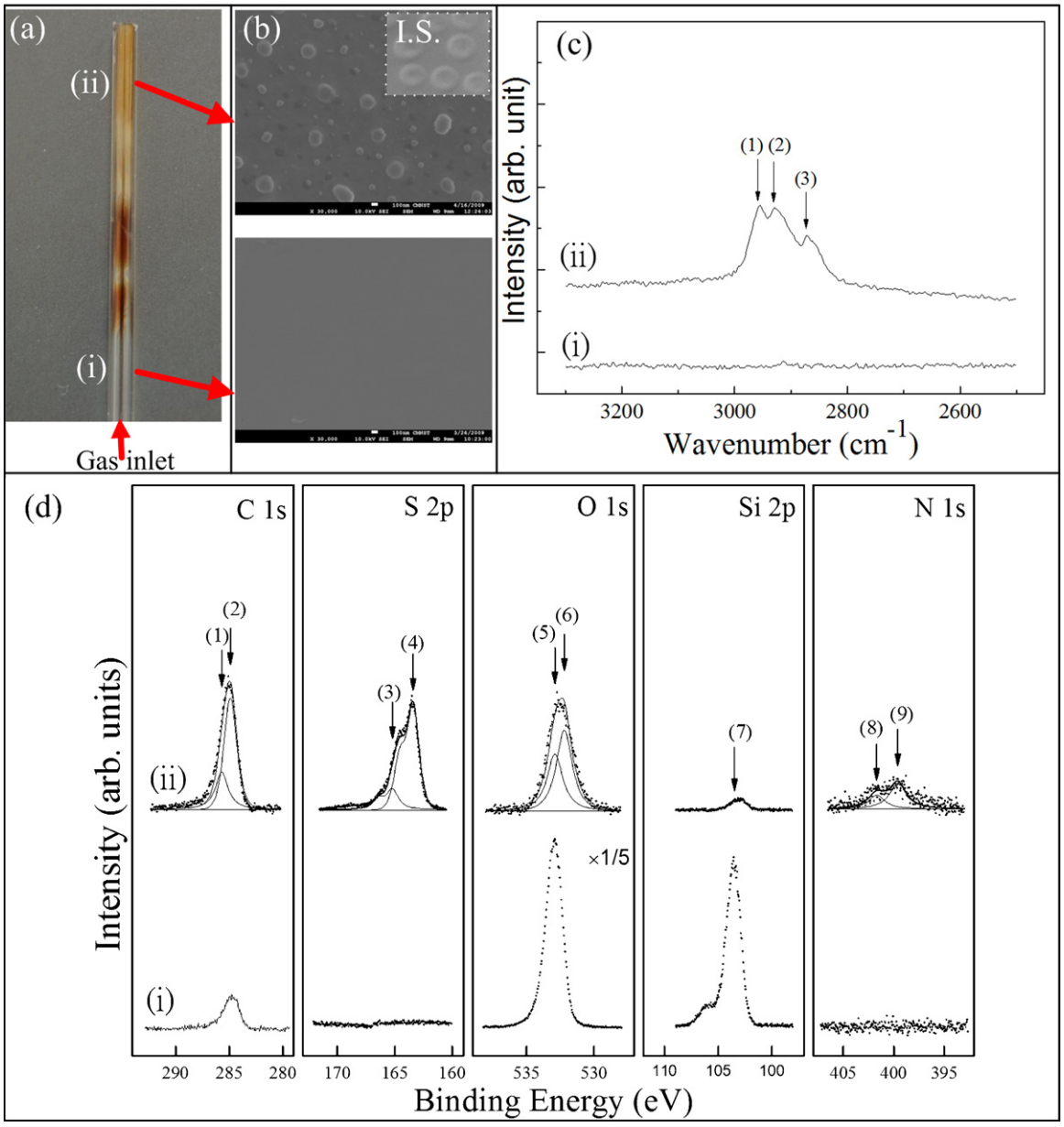

Fig. 4. (a) Appearance of quartz tube after DMS/argon micro-plasma treatment for one pair of electrodes at 40 W: zone (i) is in front of the plasma reaction zone; zone (ii) is near the afterglow region of DMS/argon plasma; (b) morphology of zone (i) and zone (i) observed using SEM (30,000×). 150–350 nm particles were deposited at initial stages (I.S.) and accumulated to form a solid film in zone (ii); (c) analysis of functional groups for zones (i) and (ii) using FTIR: the peaks exhibit IR-active modes at (1) 2954, (2) 2929, and (3) 2874 cm^{-1}, which are related to the asymmetrical CH_3 stretching, asymmetrical CH_2 stretching, and symmetrical CH_2 stretching of CH_3CH_2–S–, respectively; (d) XPS analysis for zones (i) and (ii): the peaks were assigned as (1) 285.7 (C–N), (2) 284.9 (C–C, C–H or C–S), (3) 165.2 (S–O), (4) 163.4 (S–C), (5) 532.9 (O–Si or O–N), (6) 532.2 (O–S), (7) 103.5 (Si–O), (8) 401.7 (N–O), and (9) 399.6 eV (N–C).

were introduced and reacted with active C atoms to form CO molecules due to their high thermodynamic stability (e.g., the dissociation energy, D_0 ($CO \rightarrow C + O$) = 11.2 eV, as shown in Appendix C).

The sulfide concentration as a function of the input power for the DMS/argon micro-plasma for one pair and two pairs of electrodes, respectively, was measured by GC-FPD. The concentrations of the detectable species from the reactant DMS and the products CS_2 and H_2S are shown in Fig. 3(a) and (b). The reported concentrations were obtained by comparing the calibration line with the integrated area of the characteristic sulfide peaks (data not shown). In Fig. 3(a) and (b), H_2S and CS_2 were converted by the reduction of DMS as function of input power and the extension of reaction. In Fig. 3(a), for one pair of electrodes, DMS dissociation extents were 100 (25%), 270 (67.5%), and 280 ppm (70%) for the input powers of 40, 90, and 140 W, respectively. The yields of H_2S and CS_2 increased slightly. In Fig. 3(b), for two pairs of electrodes, the DMS dissociation extent reached 100% for input powers of 90 and 140 W. From the standpoint of industrial applications, the objective is to obtain a minimum reduction of at least 98% of the VOC contained in the gas streams [17]. However, the conversion of DMS into CS_2 was much higher than that into H_2S with an increase in input power. The dissociation of DMS in argon plasma is most probably correlated with their following bond energies [11,12]: HS–H (4.0 eV), SC–S (4.5 eV), and C–S (7.4 eV).

DMS dissociation was increased by: (1) an increase of the input power for the DMS/argon micro-plasma for one pair and two pairs of electrodes, as estimated in Fig. 3(a) and (b); (2) an

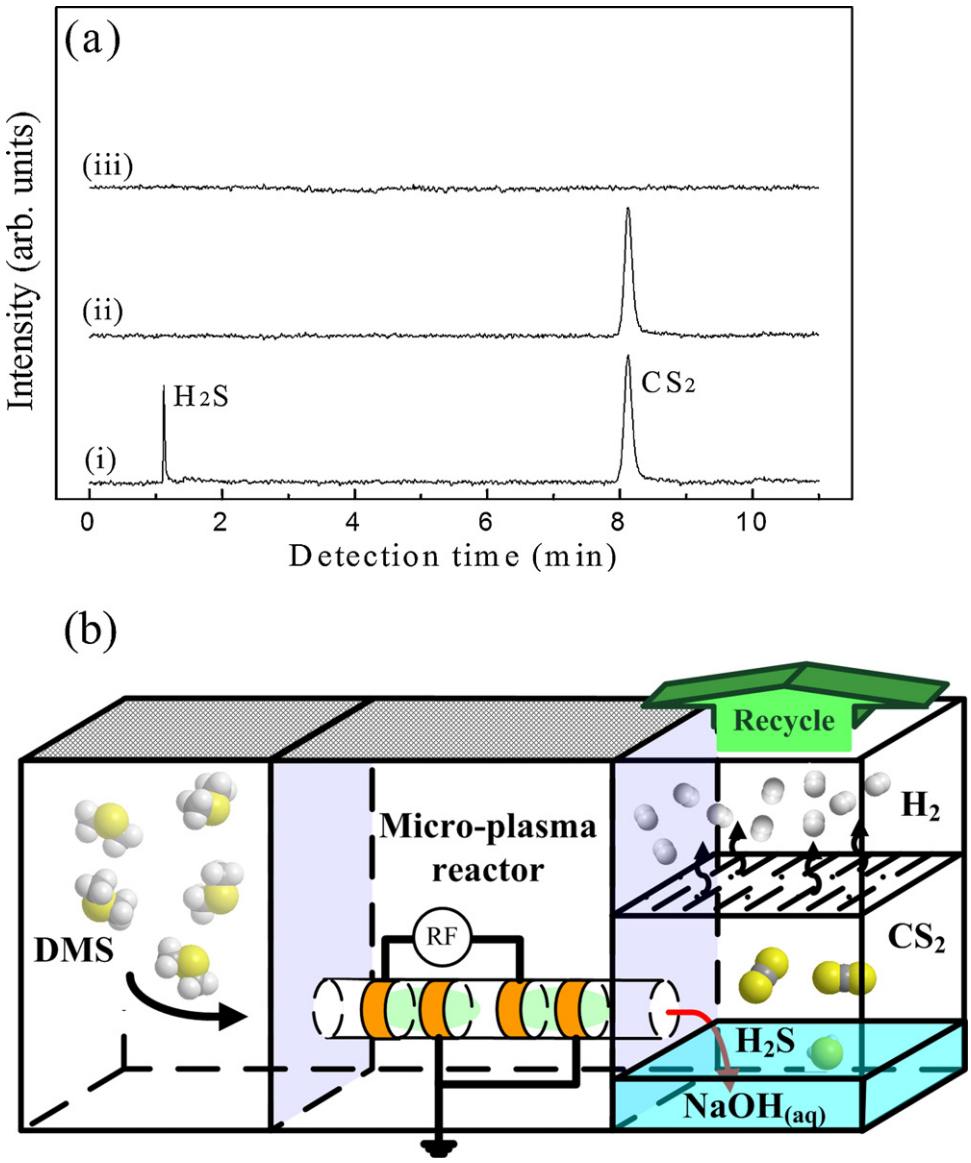

Fig. 5. (a) GC-FPD analysis of the sulfide of gaseous products after various treatments: (i) gaseous products; (ii) gaseous products treated by NaOH solution; (iii) gaseous products treated by NaOH solution and activated carbon. (b) Set-up for filtering H_2S and CS_2 and for recycling hydrogen.

increase of DMS/argon micro-plasma reaction time through the series connection of two pairs of electrodes due to complicated dissociation procedures of DMS (as shown in Appendix B). Based on the concept of activation energy in the kinetic theory, as the input power or DMS/argon plasma reaction time is increased, the probability of DMS transforming into CS_2 increases more than that of DMS transforming into H_2S. Nevertheless, the decrease of DMS and the increases of H_2S and CS_2 are not proportional, as demonstrated in Fig. 3(a) and (b). According to estimated sulfur balance, it can be found the gaseous sulfur-containing byproduct ($CS_2 + H_2S$) increases with the higher input power and longer reaction time. Further dissociation steps are described in Appendix B. Note that the estimated sulfur balance ($CS_2 + H_2S$) is incomplete, which means that other phase of sulfur byproducts should exist, even if two pairs of electrodes was applied at 140 W. Solid substance was found to deposit on the inner quartz tube in the afterglow region, as shown in Fig. 4(a) and (b). Therefore, the dissociated DMS transformed into the detectable gaseous products and solid substances.

3.3. Solid substances generated from reacted DMS/argon plasma

Yellow solid substances were found on the inner quartz tube in the afterglow region. At the initial stages, particles were gradually produced with diameters in the range of 250–350 nm, as observed by SEM (as shown in the upper-right corner of Fig. 4(b)). As shown in the upper picture in Fig. 4(b), the particles accumulated to form a solid film. EDS-SEM measurements show that the solid film was composed of C- and S-rich compounds with a ratio of 2.8 (C/S). In Fig. 4(c), the yellow solid film exhibits IR-active modes at 2954, 2929, and 2874 cm^{-1}, which are most probably related to the asymmetrical CH_3 stretching, asymmetrical CH_2 stretching, and symmetrical CH_2 stretching of CH_3CH_2–S–, respectively [25]. Note that no signal was found for a clear inner quartz tube in the range.

The chemical composition of the solid film on the inner quartz tube in the afterglow region was estimated by XPS. In Fig. 4(d), XPS spectra exhibit a pronounced increase of the elements S and C; the elements Si and O decreased due to the coverage of the solid substances on the quartz tube. The element N resulted from the

contact of the substances with the ambient air. The solid substances mostly contain the elements S and C and some N and O. In the S 2p spectra, new emission peaks related to S–C (163.4 eV for S $2p_{3/2}$) and S–O (165.2 eV) were found for the solid film. The S–C bond is related to the backbone of DMS molecules, which became fragmented and gradually deposited on the inner quartz tube in the afterglow region. The presence of the S–O bond is evidenced by the S 2p doublet (3) and O 1s peak (6) in Fig. 4(d); the bond was naturally generated due to its high electronegativity for the S-containing segment with oxygen at ambient conditions. The most probable composition of the solid substances is the backbone of $(CH_2)_n$–S, formed by the polymerization between non-dissociated DMS and reactive species, e.g., active hydrogen (H*), carbon (C*), and hydrocarbon (CH*), and some O- and N-containing products such as $(CH_2)_n$–S–O and N–$(CH_2)_n$–S. These possible products agglomerated as solid phases and precipitated on the inner quartz tube in the afterglow region. Note that the precise mass of solid substance needs further investigation for following research using nuclear magnetic resonance (NMR).

3.4. Control of DMS-free dissociation and proposal for by-product recycling

Based on the analyses of residual gases and solid substances, the increases of input power and DMS/argon reaction time tend to speed up the dissociation of DMS molecules and the recombination of the dissociated species. In general, there are four proposed mechanisms for dissociation of sulfur-containing molecule in non-thermal plasmas [12,16]: (1) direct ionization of the sulfur-containing molecule followed dissociative neutralization (e.g., $e + DMS \rightarrow DMS^+ + 2e$, $DMS^+ + 2e \rightarrow CH_3S^* + CH_3^*$); (2) ionization of the buffer gas, leading to charge transfer reaction, and subsequent dissociative neutralization (e.g., $e + Ar \rightarrow Ar^+ + 2e$, $Ar^+ + DMS \rightarrow DMS^+ + Ar$, $DMS^+ + 2e \rightarrow CH_3S^* + CH_3^*$); (3) direct electron collision dissociation (e.g., $e + DMS \rightarrow CH_3S^* + CH_3^* + e$); (4) excitation of the buffer gas, which produces active species that contribute to the sulfur-containing molecule (e.g., $e + Ar \rightarrow Ar^* + e$, $Ar^* + DMS \rightarrow CH_3S^* + CH_3^* + Ar$). The energy cost of electron detachment (first ionization energy) in DMS and in argon is 8.69 eV [7] and 15.8 eV [16] respectively which is much higher than the energy of bond dissociation (shown in Appendix B), which resulted from direct electron collision or the excited (or metastable) argon species (the energy carried by the argon metastables Ar (4s) is around 11.5–11.7 eV). Therefore, the pathways (3) and (4) are most probable for DMS conversion in the present study. The increase of DMS/argon reaction time results in the further dissociation steps and the enhancement of recombining the dissociated species.

In addition, managing the by-products is a critical issue. In this work, the solid substances can be left on the quartz tube in the afterglow region, whereas the decomposed gases should be collected and treated. By-products H_2, H_2S, and CS_2 are produced in the afterglow region. $NaOH_{(aq)}$ was employed to convert $H_2S_{(g)}$ to $NaHS_{(aq)}$ and $H_2O_{(l)}$. In Fig. 5(a) (i) and (ii), $H_2S_{(g)}$ was completely dissolved after this procedure. The concentrated $NaHS_{(aq)}$ can be used as a reagent for the synthesis of organic/inorganic compounds [26]. An activated carbon filter was then applied to trap $CS_{2(g)}$, as indicated in Fig. 5(a) (iii). The activated carbon filter can be recycled by following a regeneration procedure (e.g., a thermal method) [27]. The extremely low-concentration $CS_{2(g)}$ can then be collected and treated. Most hydrogen can pass through $NaOH_{(aq)}$ and activated carbon and recycled as an energy resource. Fig. 5(b) shows the proposed recycling procedures for H_2S, CS_2, and hydrogen.

4. Conclusion

A custom-made atmospheric argon micro-plasma system was employed to dissociate DMS into non-foul-smelling species. DMS is converted into recombined gases and solid substances; a complete dissociation of DMS can be achieved. The increases of input power and DMS/argon reaction time tend to speed up the dissociation of DMS molecules and the recombination of the dissociated species. The solid by-products can be left on the quartz tube in the afterglow region, whereas the gaseous by-products should be treated (e.g., dissolved into aqueous solution or trapped in an activated carbon filter). Through this treatment, the conversion of DMS is presumably an eco-friendly process. An array of micro-plasma reactors can be furthermore considered for mass treatment in company with recyclable gaseous by-products.

Acknowledgements

This work was financially supported by Chi-Mei Optoelectronics (under grant number 97S062) and National Science Council of Taiwan (under grant numbers 99-2221-E-006-013-MY3, 99-2911-I-006-013-, and 100-2911-I-006-008-).

Appendix A.

See Table 1.

Appendix B.

Most of the decompositions in DMS/argon plasma and subsequent reactions are listed as Eqs. (1)–(11). Excited CH_3S^* (Eq. (A.1)) can be decomposed into CH_2S, CHS, CS, CH_2, CH_3, CH, H, and S (Eqs. (A.3)–(A.11)), where D_0 is the bond dissociation energy (units: eV) [11].

CH_3SCH_3 (DMS) + e- (or Ar^*) → $CH_3S^* + CH_3^*$	$D_0 = 3.3$ eV (A.1)
CH_3SCH_3 (DMS) + e- (or Ar^*) → $CH_3SCH_2^* + H^*$	$D_0 = 4.0$ eV (A.2)
$CH_3S^* \rightarrow CH_2S^* + H^*$	$D_0 = 2.1$ eV (A.3)
$CH_2S^* \rightarrow CHS^* + H^*$	$D_0 = 4.1$ eV (A.4)
$CHS^* \rightarrow CS^* + H^*$	$D_0 = 2.0$ eV (A.5)
$CS^* \rightarrow C^* + S^*$	$D_0 = 7.4$ eV (A.6)
$CH_2S^* \rightarrow CH_2^* + S^*$	$D_0 = 5.7$ eV (A.7)
$CH_3S^* \rightarrow CH_3^* + S^*$	$D_0 = 3.0$ eV (A.8)
$CH_3^* \rightarrow CH_2^* + H^*$	$D_0 = 4.6$ eV (A.9)
$CH_2^* \rightarrow CH^* + H^*$	$D_0 = 4.8$ eV(A.10)
$CH^* \rightarrow C^* + H^*$	$D_0 = 4.3$ eV(A.11)

Appendix C.

A Fourier transform infrared spectrometer (FTIR, Nexus 470, *Thermo Nicolet*, USA) combined with a transmittance-type 9.6 m gas cell was applied to analyze the variation of gaseous products after

Table 1
Plasma parameters for gaseous-pollution-control atmospheric-pressure plasma sources [7,9,13,14,17–19,28].

Plasma source	Plasma density (cm^{-3})	Gas temperature	Energy density (J/cm^3)	V_b[a] (kV)
Plasma torch	10^{16}–10^{19}	Extremely high	700–1200	10–50
Barrier discharge	10^{12}–10^{15}	Low	0.16–1.6	5–25
Pulsed corona	10^{9}–10^{13}	Low	0.1–0.3	10–50
Micro-plasma	10^{11}–10^{12}	Low	0.5–3	0.05–0.2

[a] V_b: Breakdown voltage.

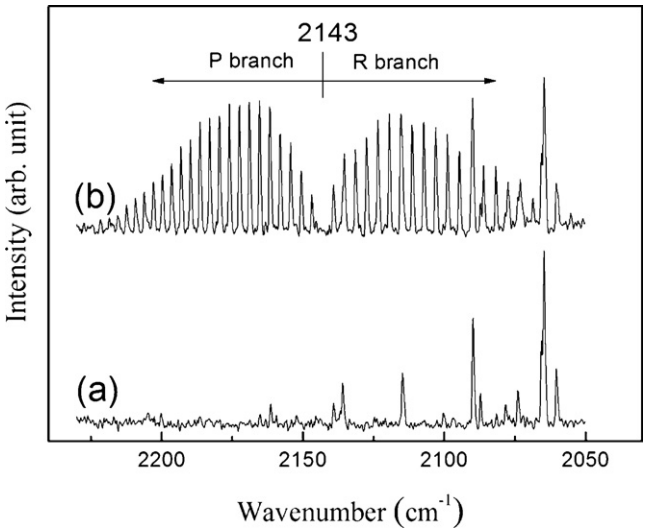

Fig. C1. Gaseous products after (a) argon and (b) DMS/argon micro-plasma treatment using a one pair of electrodes at 40 W detected by FTIR.

DMS/argon micro-plasma treatment. In Fig. C1, P- and R- branches (e.g., centered at about 2143 cm^{-1}) of carbon monoxide (CO) can be observed. This implies that a small number of active O atoms from the atmosphere were introduced and reacted with active C atoms to form CO molecules due to their high thermodynamic stability (e.g., the dissociation energy, D_0 ($CO \rightarrow C + O$) = 11.2 eV).

References

[1] R. Bentley, T.G. Chasteen, Environmental VOSCs – formation and degradation of dimethyl sulfide, methanethiol and related materials, Chemosphere 55 (2004) 291–317.
[2] C.N. Lei, L.M. Whang, H.L. Lin, Biological treatment of thin-film transistor liquid crystal display (TFT-LCD) wastewater, Water Science and Technology 58 (2008) 1001–1006.
[3] R. Simo, Trace chromatographic analysis of dimethyl sulfoxide and related methylated sulfur compounds in natural waters, Journal of Chromatography A 807 (1998) 151–164.
[4] J.J. Wu, M. Muruganandham, S.H. Chen, Degradation of DMSO by ozone-based advanced oxidation processes, Journal of Hazardous Materials 149 (2007) 218–225.
[5] H. Chu, W.T. Lee, K.H. Horng, T.K. Tseng, The catalytic incineration of (CH3)(2)S and its mixture with CH3SH over a Pt/Al_2O_3 catalyst, Journal of Hazardous Materials 82 (2001) 43–53.
[6] J.R. Kastner, K.C. Das, N.D. Melear, Catalytic oxidation of gaseous reduced sulfur compounds using coal fly ash, Journal of Hazardous Materials 95 (2002) 81–90.
[7] J. Jarrige, P. Vervisch, Decomposition of gaseous sulfide compounds in air by pulsed corona discharge, Plasma Chemistry and Plasma Processing 27 (2007) 241–255.
[8] M. Leins, L. Alberts, M. Kaiser, M. Walker, A. Schulz, U. Schumacher, U. Stroth, Development and characterisation of a microwave-heated atmospheric plasma torch, Plasma Processes and Polymers 6 (2009) S227–S232.
[9] M. Nantel-Valiquette, Y. Kabouzi, E. Castanos-Martinez, K. Makasheva, M. Moisan, J.C. Rostaing, Reduction of perfluorinated compound emissions using atmospheric pressure microwave plasmas: mechanisms and energy efficiency, Pure and Applied Chemistry 78 (2006) 1173–1185.
[10] C.H. Tsai, W.J. Lee, C.Y. Chen, W.T. Liao, Decomposition of CH3SH in a RF plasma reactor: reaction products and mechanisms, Industrial & Engineering Chemistry Research 40 (2001) 2384–2395.
[11] C.H. Tsai, W.J. Lee, C.Y. Chen, W.T. Liao, M. Shih, Formation of solid sulfur by decomposition of carbon disulfide in the oxygen-lean cold plasma environment, Industrial & Engineering Chemistry Research 41 (2002) 1412–1418.
[12] C.H. Tsai, W.J. Lee, C.Y. Chen, P.J. Tsai, G.C. Fang, M.L. Shih, Difference in conversions between dimethyl sulfide and methanethiol in a cold plasma environment, Plasma Chemistry and Plasma Processing 23 (2003) 141–157.
[13] J.S. Chang, Recent development of plasma pollution control technology: a critical review, Science and Technology of Advanced Materials 2 (2001) 571–576.
[14] C. Subrahmanyam, A. Magureanu, A. Renken, L. Kiwi-Minsker, Catalytic abatement of volatile organic compounds assisted by non-thermal plasma – Part 1. A novel dielectric barrier discharge reactor containing catalytic electrode, Applied Catalysis B-Environmental 65 (2006) 150–156.
[15] S.E. Park, R. Ryoo, W.S. Ahn, C.W. Lee, J.S. Chang, Nanotechnology in Mesostructured Materials, 1st ed., Elsevier, Amsterdam, 2003.
[16] G.B. Zhao, S. John, J.J. Zhang, J.C. Hamann, S.S. Muknahallipatna, S. Legowski, J.F. Ackerman, M.D. Argyle, Production of hydrogen and sulfur from hydrogen sulfide in a nonthermal-plasma pulsed corona discharge reactor, Chemical Engineering Science 62 (2007) 2216–2227.
[17] M.G. Sobacchi, A.V. Saveliev, A.A. Fridman, A.F. Gutsol, L.A. Kennedy, Experimental assessment of pulsed corona discharge for treatment of VOC emissions, Plasma Chemistry and Plasma Processing 23 (2003) 347–370.
[18] R. Foest, M. Schmidt, K. Becker, Microplasmas, an emerging field of low-temperature plasma science and technology, International Journal of Mass Spectrometry 248 (2006) 87–102.
[19] A.D. Koutsospyros, S.M. Yin, C. Christodoulatos, K. Becker, Destruction of hydrocarbons in non-thermal, ambient-pressure, capillary discharge plasmas, International Journal of Mass Spectrometry 233 (2004) 305–315.
[20] A.D. Koutsospyros, S.M. Yin, C. Christodoulatos, K. Becker, Plasmochemical degradation of volatile organic compounds (VOC) in a capillary discharge plasma reactor, IEEE Transactions on Plasma Science 33 (2005) 42–49.
[21] L.A. Rosocha, Y. Kim, Application of non-thermal plasmas to gas cleaning and enhancing combustion pollution reduction, in: International Conference on Air Pollution Abatement Technologies-Future Challenges, Queensland, Australia, 2006, Paper 5C2.
[22] H.H. Chen, C.C. Weng, J.D. Liao, K.M. Chen, B.W. Hsu, Photo-resist stripping process using atmospheric micro-plasma system, Journal of Physics D: Applied Physics 42 (2009).
[23] R.W.B. Pearse, A.G. Gaydon, The Identification of Molecular Spectra, 4th ed., Chapman and Hall, London, 1976.
[24] Q. Xiong, A.Y. Nikiforov, X.P. Lu, C. Leys, High-speed dispersed photographing of an open-air argon plasma plume by a grating-ICCD camera system, Journal of Physics D: Applied Physics 43 (2010).
[25] G. Socrates, Infrared and Raman Characteristic Group Frequencies: Tables and Charts, 3rd ed., Wiley, Chichester, 2004.
[26] A.R. Siekkinen, J.M. McLellan, J.Y. Chen, Y.N. Xia, Rapid synthesis of small silver nanocubes by mediating polyol reduction with a trace amount of sodium sulfide or sodium hydrosulfide, Chemical Physics Letters 432 (2006) 491–496.
[27] J.C. Enneking, Control of carbon disulfide emissions from viscose processes, Environmental Progress 21 (2002) 169–174.
[28] A. Schütze, J.Y. Jeong, S.E. Babayan, J. Park, G.S. Selwyn, R.F. Hicks, The atmospheric-pressure plasma jet: a review and comparison to other plasma sources, IEEE Transactions on Plasma Science 26 (1998) 1685–1694.